

Spectroscopic and coarse-grained simulation studies of the BSA and HSA protein adsorption on silver nanoparticles

Mariana Voicescu · Sorana Ionescu ·
Daniel G. Angelescu

Received: 26 March 2012 / Accepted: 30 August 2012
© Springer Science+Business Media B.V. 2012

Abstract The photophysical properties of the bovine serum albumin (BSA) and human serum albumin (HSA) adsorbed on (non) functionalized Ag(0) nanoparticles have been studied by spectroscopic techniques. The surface plasmon resonance kinetic of the BSA/HSA-Ag(0) nanoparticle complexes has been assessed by UV–Vis absorption spectroscopy. Transmission electron microscopy analysis showed that the average size of the particles is ~ 9 nm and the core–shell structure of the protein-Ag(0) nanoparticle complexes has been supported by UV–Vis spectra. The structure, stability, dynamics, and conformation of the proteins have been investigated by steady-state, time-resolved fluorescence, and circular dichroism spectroscopy. Insights of the HSA conformation at the nanoparticle surface were obtained by the Monte Carlo simulations carried out using an appropriate coarse-grained model. The HSA conformation upon adsorption on the nanoparticle surface is distorted so that the Trp fluorescence is quenched and the α -helix content diminished. The adsorbed protein exhibited an

extended conformation with Trp residue depleted from the nanoparticle surface and rather located toward the protein boundary. Experimental and simulated experiments were in good agreements and the results are discussed in terms of functional properties of the serum albumins in protein–Ag(0) nanoparticle complex.

Keywords Silver nanoparticles · Proteins · Fluorescence · Monte Carlo simulations

Introduction

The speed of development of nanoscience is well known, however, relatively little is known about the effect of the surface chemistry of nanoparticles on the biomolecules adsorption that presents a serious problem in the whole nanomedicine and nanotoxicology. It was reported that, in most cases, the biomolecules, especially proteins, undergo some structural changes at the boundary surface of nanoparticles (Roach et al. 2006).

Integrating biological molecules with nanoparticles permits to combine natural biomolecule functions, such as catalysis, recognition, and electron transfer, with the unique electronic, optical and catalytic properties of nanoparticles, arising from their reduced dimension and high surface-to-volume ratio (Niemeyer 2001; Gu et al. 2006; Huo 2007). It was reported that

M. Voicescu (✉) · D. G. Angelescu
Institute of Physical Chemistry “Ilie Murgulescu”
of the Romanian Academy, Splaiul Independentei 202,
060021 Bucharest, Romania
e-mail: voicescu@icf.ro

S. Ionescu
Department of Physical Chemistry,
University of Bucharest, Bd Regina Elisabeta 4-12,
030018 Bucharest, Romania

when biomolecules are conjugated with nanoparticles, the mixing of their energy levels has been shown to favor the occurrence of either energy transfer or electron transfer phenomena (Lakowicz et al. 2003; Willner et al. 2007). In this way, it is possible to study fundamental processes characterizing the interaction of metal nanoparticles with biological molecules (Link and El-Sayed 2000; Jain et al. 2007a, b; Jensen et al. 2005; Hayat 1991; Allara 1995; Ulman 1991, 1996). The particles have a characteristic plasmon absorbance when the core diameter is larger than 2 nm and the plasmon absorbance is sensitive to the surrounding medium and expected to change when the particles are aggregated (Ingram et al. 1997; Templeton et al. 1998, 2000; Hostetler et al. 1999; Esumi et al. 1995; Link et al. 1999); The size of nanoparticles being similar to that of most biological molecules and structures, it can be of immense importance for both in vivo and in vitro biomedical research and applications. In this account, biophysical studies of the noble metals (Sönnichsen et al. 2005; Reinhard et al. 2007; Jain et al. 2006, 2008) as well as their applications in imaging (Sokolov et al. 2003; El-Sayed et al. 2005; Alivisatos 2004), biological sensing (Elghanian et al. 1997; Haes and Van Duyne 2002), medical diagnostics (Rosi and Mirkin 2005), and cancer medical treatment (Huang et al. 2006, 2007; El-Sayed et al. 2006; O'Neal et al. 2004; Jain et al. 2007a, b; Wang et al. 2010), have been reported.

Recently, it was shown that silver nanoparticles (SNPs) with antibacterial activity are used to treat burn wounds (Tian et al. 2007), as coatings in surgical masks (Li et al. 2006), in implantable devices (Furno et al. 2004), as biosensors to detect *E. coli* in apple and milk juice (Naja et al. 2010). SNPs have antiplatelet properties useful in the treatment of thrombotic disorders (Shrivastava et al. 2009). The interaction of SNPs with the proteins present in plasma is of major importance in biomedical applications of nanoparticles and in the growing biosafety of nanomaterials.

The biological functions of albumins, mostly based on their ability to carry drugs as well as endogenous and exogenous substances, are well known (Moreno et al. 1999; Olson and Christ 1996). As water soluble proteins, serum albumins are the most abundant proteins present in plasma and among these, bovine serum albumin (BSA) and human serum albumin (HSA) were found to bind reversibly a huge number of compounds as well as to present a wide range of

physiological functions involving delivery of fatty acids, metabolic products like thyroxine, porphyrins, bilirubin, and steroids. In these regards it was reported that the sulfhydryl groups present in BSA are scavengers of reactive oxygen and nitrogen species, with an important role in oxidative stress (Evans 2002; Hansen 1981; Valanciunaite et al. 2006).

BSA and HSA with a polypeptide chain of 582 and 585 amino acids residues, respectively, are different in Tryptophan (Trp) numbering and localization. BSA has two Tryptophan (Trp) residues involved in its intrinsic fluorescence: Trp212 which belongs to subdomain IIA within a hydrophobic binding pocket and Trp134 which belongs to the first subdomain IB, located on the surface of the albumin molecule. HSA contains only one Trp residue, Trp214, located within the hydrophobic pocket in subdomain IIA, Sudlow site I (Sudlow et al. 1976).

Studies on the interaction between Ag ion and colloidal SNPs with BSA have been recently reported (Zhao et al. 2011; Ravindran et al. 2010). It was found that the BSA adsorption on the surface prevented the Ag nanoparticles from aggregating in solutions of pH greater than 5. At basic pH, changes in BSA conformational structure upon its interaction with SNPs, was evidenced. It was found that the aggregation of the SNPs prevents their uptake in live cells and limits their applicability as bioprobes (Ravindran et al. 2010). The energy transfer distance from Trp212 of BSA to Ag was found to be 10 nm (Zhao et al. 2011). The intrinsic fluorescence of BSA bound to SNPs was quenched by both static and dynamic quenching mechanism, the protein exhibiting at the same time an enhanced hydrophobicity (Mariam et al. 2011).

In this paper, the photophysical properties of the BSA and HSA adsorbed on (non) functionalized Ag(0) nanoparticles are investigated. The plasmonic features of the BSA/HSA–Ag(0) nanoparticle complexes as a function of time and temperature will be also investigated by UV–Vis absorption spectroscopy. Using steady-state and time resolved fluorescence spectroscopy, the structure, stability, and dynamics of the proteins will be studied. By circular dichroism spectroscopy, the conformational changes of the adsorbed proteins is also considered. Complementary information regarding the conformation adopted in the adsorbed state will be obtained by Monte Carlo simulations carried out on a simple coarse-grained model with focus on electrostatic interactions between

the SNPs and the HSA protein. The results related to the functional properties of the serum albumins in protein–Ag(0) nanoparticle complex are discussed.

Experimental

Materials

The silver source, silver nitrate (AgNO_3 , purity 99.99 %), and the reducing agent, sodium borohydride (NaBH_4 , purity 99.8 %) were purchased from Sigma-Aldrich. SNPs were prepared accordingly to Angelescu et al. 2010, by adding under vigorous stirring appropriate aliquots of 1 mM AgNO_3 solution to a solution-containing NaBH_4 so that their final concentrations were 0.1 mM AgNO_3 and 7 mM NaBH_4 , respectively. No capping agent was needed as the resulting nanoparticles were electrostatically stabilized (Angelescu et al. 2010). To this aqueous solution, varying concentrations of BSA or HSA proteins in the range $1.65\text{--}3.30 \times 10^{-5}$ M were added. BSA and HSA were purchased from Merck and used without further purification.

Methods and apparatus

Transmission electron microscopy specimens were prepared by placing droplets of the aqueous solution-containing bare Ag nanoparticles onto carbon-coated TEM grid and letting subsequently evaporation of the solvent under ambient conditions. The as-synthesized nanoparticles were visualized using a transmission electron microscope model JEM 200CX equipped with a KeenView CCD camera and operating at 120 kV.

The absorption measurements were recorded using a Perkin Elmer, Lambda 35, UV–Vis Spectrometer at a scan rate of 480 nm min^{-1} and a spectral resolution of 0.5 nm.

The fluorescence emission spectra were recorded with a Jasco FP-6500 Spectrofluorometer equipped with a 450 W Xenon Lamp, using 3 nm band passes for the excitation and the emission monochromators, the detector response of 1 s, data pitch of 0.5 nm. The excitation wavelength was 280 nm.

The fluorescence decays measurements were performed by using the time-correlated single-photon counting (TCSPC) technique. The excitation source

was an electroluminescent diode (NanoLED-295, Model EP LED 295, Edinburgh Instruments FLS 920), emitting at 295 nm with a bandwidth of 10 nm and giving pulses of 762.7 ps. The NanoLED diode operated at 1 MHz repetition rate, Delay 5 ns, TAC Range 50 ns, 18 nm band pass. The decay curves were stored in 1,024 channels of 0.049 ns/ch. The NanoLED pulse was recorded using a diluted Ludox solution. To determine the fluorescence lifetime of the compounds, the fluorescence decay data were fitted with a multiexponential function with two or three components

$$F(t) = \alpha_1 \exp(-t/\tau_1) + \alpha_2 \exp(-t/\tau_2) + \alpha_3 \exp(-t/\tau_3) \quad (1)$$

and the fit was checked on grounds of χ^2 .

$\langle \tau \rangle$, the average fluorescence lifetimes were calculated from the following relation (Lakowicz 1999):

$$\langle \tau \rangle = \frac{\sum_i \alpha_i \tau_i^2}{\sum_i \alpha_i \tau_i} \quad (2)$$

Circular dichroism analysis

The circular dichroism spectra were carried out on a Jasco J-815 spectropolarimeter on solutions containing of 0.044 mg/mL of BSA/HSA proteins, in the wavelength range of 200–300 nm. The program package CDfit (Rupp <http://www.ruppweb.org>) was used to analyze the detailed secondary structure changes.

Model system and Monte Carlo simulations

The conformation adopted by the HSA molecule at the Ag(0) nanoparticle surface has been investigated by performing Monte Carlo simulations on a so-called coarse-grained model. Despite the fact that the degrees of freedom of the protein were reduced as compared with all-atom molecular model, rendering thus the coarse graining less predictive than all-atoms simulations, one considers that the coarse graining permitted computational investigations about the key physical details governing the large-scale protein conformation in the presence of Ag nanoparticles (Tozzini 2005; Lund and Jönsson 2003). As usually considered in polyelectrolyte simulation studies (Jonsson et al. 2003; Akinchina and Linse 2002; Angelescu et al. 2007; Skepo et al. 2006), the atomistic structure of the HSA

polyelectrolyte was coarse-grained and surrounding medium entered the model as a continuum dielectric of constant relative permittivity. Each amino acid was represented by a single bead, and the beads were connected by harmonic bonds into a freely jointed linear chain. The secondary structure and the disulfide bonds were not taken into consideration by the present model, yet we consider that such a simple protein model should still describe the main coarse-grained features of the HSA protein adsorption onto Ag(0) nanoparticles. The beads were represented as hard spheres of radius $R_{aa} = 2 \text{ \AA}$, and they bore additional features in line with amino acid sequence of HSA protein (PDB file:1AO6). Thus, the beads had positive or negative charge or they were neutral. The modeled protein had a net charge of $-23e$, arising from 122 negatively charged, 99 positively charged, and 364 uncharged amino acids. For the last ones the hydrophobicity scale was additionally considered, and a non-electrostatic attractive potential, $U_{\text{short}} \sim \varepsilon r^6$, was assigned to the most hydrophobic uncharged amino acids. For the sake of simplicity, an average value $\varepsilon = 1.23 kT$ for Ala, Met, Leu, Val, Ile, Phe amino acids was used.

As to the Ag(0) nanoparticles, their curvature was neglected and the flat surface bore discrete positively charged sites located 2 \AA beneath the surface and arranged in a 2D quadratic lattice. The considered surface potential of 40 mV was in accordance with the zeta-potential of bare Ag(0) nanoparticles experimentally reported (Abdullin et al. 2010). The counter ions to insure the electro-neutrality of the HSA-surface system were included explicitly as well. The charged species were all enclosed in a rectangular box exhibiting two hard walls along z direction and the periodic boundary conditions were applied in the other two directions. The parameters used for modeling the HSA protein at the oppositely charged surface are summarized in Table 1.

All interactions in the system were taken as pairwise additive. The total potential energy U of the system is given by

$$U = U_{\text{nonbond}} + U_{\text{bond}} + U_{\text{angle}} + U_{\text{ext}} \quad (3)$$

The first term can be expressed as a sum of hard-sphere interactions and electrostatic potential according to

$$U_{\text{nonbond}} = \sum_{i < j} u_{ij}(r_{ij}) = \begin{cases} \infty, & r_{ij} < R_i + R_j \\ \sum_{i < j} \frac{Z_i Z_j e^2}{4\pi\epsilon_0\epsilon_r r_{ij}} - \sum_{i,j} 4\varepsilon_{ij} \left(\frac{1}{r_{ij}}\right)^6, & r_{ij} \geq R_i + R_j \end{cases} \quad (4)$$

where r_{ij} is the distance between the centers of particles i and j (amino acid, counter ions, or surface sites), Z_i and R_i the charge and the radius of the mobile particle i , e the elementary charge, ϵ_0 the permittivity of the vacuum, ϵ_r the relative permittivity of the solvent. ε_{ij} define the attractive potential between the hydrophobic amino acids i and j .

The second- and third-term of Eq. 3, the bond energy U_{bond} , and the angular energy, U_{angle} , are the harmonic potentials connecting two amino acid units and modeling the chain stiffness (Angelescu et al. 2007). The last term U_{ext} in Eq. 3 describes the confining cell potential in z direction, and it is given by

$$U_{\text{cell}} = \sum_i u_{\text{cell}}(r_i) = \begin{cases} 0, & -z_w < r_i < z_w \\ \infty, & \text{otherwise} \end{cases} \quad (5)$$

The Monte Carlo simulations were performed in the canonical ensemble employing the standard Metropolis algorithm. Four kinds of trial displacement were employed for the protein: (i) single bead move, (ii) pivot rotation of a randomly selected protein chain section, (iii) translation of the entire protein chain, and (iv) slithering move. The long-range electrostatic interactions were calculated using Ewald summation with extension to the slab geometry. Simulations were all carried using the integrated Monte Carlo/molecular dynamics/Brownian dynamics simulation package MOLSIM (Linse 2009).

Results and discussion

Transmission electron microscopy

The Ag(0) nanoparticle prepared in the absence of any stabilizing agent did not exhibit any changes in the plasmon resonance band for at least 3 months. They were electrostatically stabilized as they precipitated easily upon addition of 0.1 M monovalent salt (Angelescu et al. 2010). A TEM image of the bare Ag nanoparticles, prior to the protein addition is

Table 1 Data of the simulated system

<i>Simulation box</i>	
Box size	600 Å × 600 Å × 700 Å
External walls	$z_w = \pm 300$ Å
Relative permittivity	$\epsilon = 78.4$
Temperature	$T = 298$ K
<i>HSA protein</i>	
Amino acid radius	$R_{aa} = 2$ Å
Amino acid charge	$Z_{aa} = -1, 0, +1$ e
Amino acid number	
Positively charged	122 ^a
Negatively charged	99 ^b
Neutral	155 ^c
Hydrophobic	209 ^d
Short-range attractive parameter	$\epsilon = 1.23$ kT
<i>Ag surface</i>	
Location	$z_s = -302$ Å
Surface charge density	$\sigma_s = 0.0013$ e Å ^{-2e}
Surface charge spacing	$d_s = 30$ Å
Number of sites	$n_s = 400$
<i>Small ions</i>	
Small ion radius	$R_{ion} = 2$ Å
Small ion charge	$Z_{ion} = -1$ e
Small ion number	$n_{ion} = 444$

^a Asp, Glu, Ser

^b Arg, Lys, His

^c Asn, Gln, Tyr, Thr, Gly, Cys, Pro, Trp

^d Ala, Met, Leu, Val, Ile, Phe

^e The surface potential is 40 mV

shown in Fig. 1. It is seen that two populations represented by individual and networked nanoparticles coexisted. The clusters were given by linked entities with an apparent diameter in 4–20 nm range, whereas the mean size of the individual nanoparticles amounted to 9 nm.

UV–Vis absorption measurements

Absorption spectrum of BSA–Ag(0) nanoparticle complex as a function of time is shown in the Fig. 2a. The bare Ag(0) nanoparticles exhibited the plasmon resonance characterized by an absorption band centered at 383 nm. Upon BSA addition, an absorption band around 277 nm appeared. This band is corresponding to π – π^* transition of aromatic amino acid residues, Tyr and Trp (Voicescu et al. 2009a, b). At the

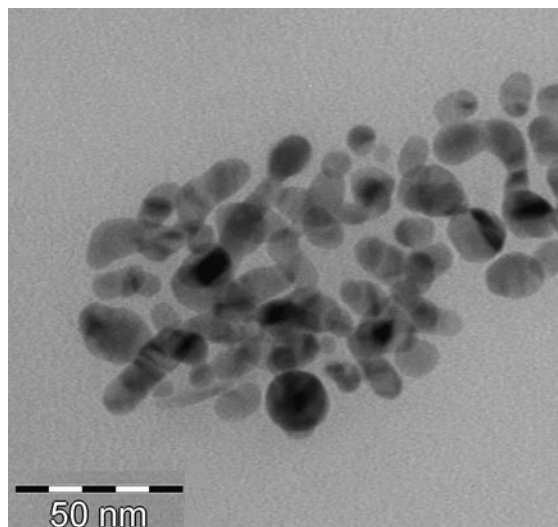
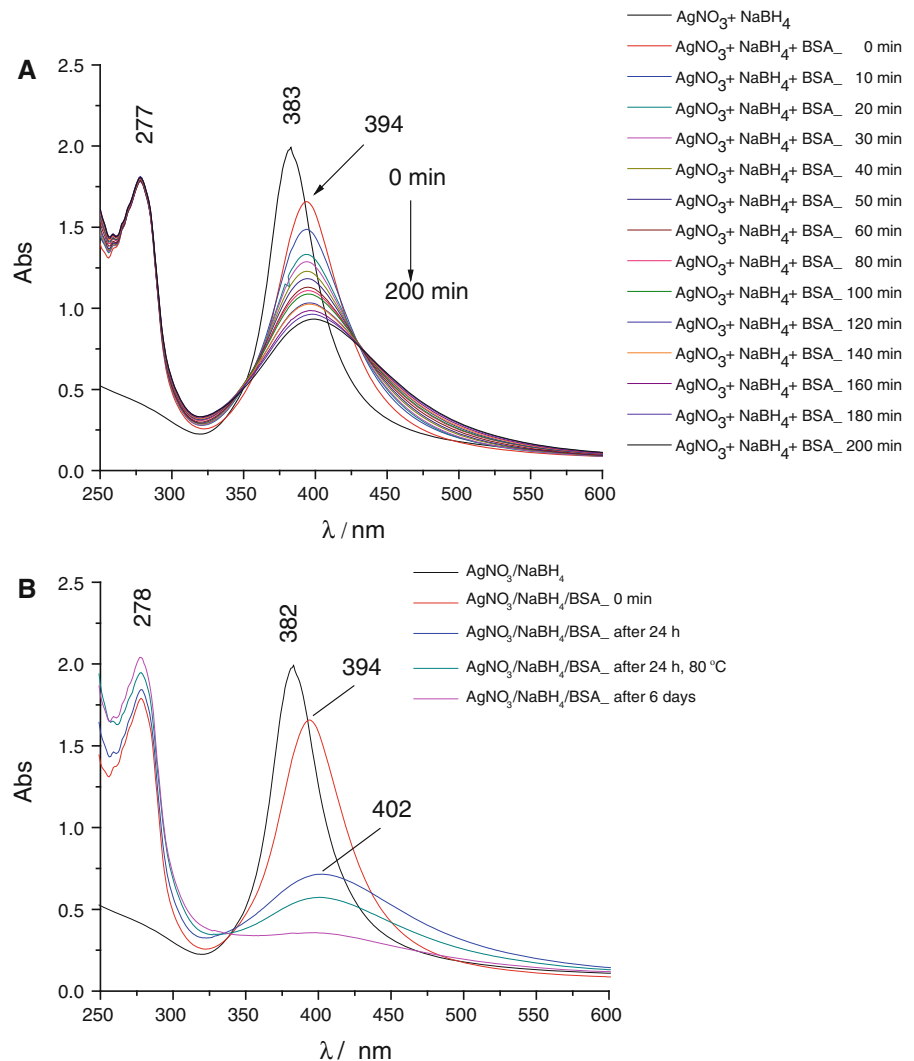


Fig. 1 TEM micrograph of Ag nanoparticles prior to the protein addition

same time, the Ag(0) nanoparticle plasmon band is shifted from 383 to 394 nm initially. Then, in long run, a bathochromic shift from 394 to 402 nm of the maximum wavelength associated with an intensity decrease and band broadening occurred (Fig. 2a,b). Note also that the changes of the nanoparticle plasmon band did not lead to distortions of the Tyr and Trp residues absorption at 277 nm. The lack of any change in this absorption band at 277 nm implies the probable dynamic quenching mechanism of the BSA fluorescence by Ag⁺. As to the Ag(0) nanoparticles plasmon band, its time-dependent behavior is attributed to the protein adsorption on the Ag(0) nanoparticles surface since the nanoparticles grew to their full completion prior to the protein addition (see Experimental section). The time evolution of absorption band can be understood in terms of the plasmonic properties of a metal–dielectric core–shell nanoparticle. Thus, shortly after protein addition, the adsorption occurs at high rates and the protein–nanoparticle complex can be envisaged as a core–shell structure where the core Ag(0) nanoparticle is surrounded by a dielectric shell of adsorbed protein molecules whose refractive index is larger than that of the bulk solution. Once the protein accumulates at the surface, it undergoes conformational changes, as suggested by the simulation studies presented in the next section. Furthermore, the subsequent attachment process is limited by an electrostatic and steric barrier so that the adsorption

Fig. 2 UV–Vis absorption spectra of the BSA–Ag(0) nanoparticle complex at different reaction time (a) and time–temperature (b). The concentration of BSA is 3.29×10^{-5} M



rate gradually decreases and a plateau is reached. Based on this assumption, one expects the plasmon band of the protein-coated nanoparticle to be red shifted as compared with bare nanoparticles (Amendola et al. 2010) and the process kinetic to resemble the adsorption kinetic of the charged polymers onto oppositely charged surface (Samoshima et al. 2005).

The same effect is also observed after 24 h under temperature treatment, 80°C , respectively (Fig. 2b). After 6 days, the plasmon resonance band is completely affected. In this last case, besides the monodispersity of the Ag(0) nanoparticles, BSA could cause strong hydrophobic interactions with Ag(0)

nanoparticles. The increase in the absorption band at 278 nm, leads to the supposition that BSA might have changes in its conformation.

Figure 3 shows the UV–Vis absorption spectrum profiles of the HSA–Ag(0) nanoparticle complex as function of reaction time and temperature. One sees that the plasmon band exhibits similar behavior as that previously reported in case of BSA–Ag(0) nanoparticle complex. In more details, the wavelength at the absorption peak, λ_{max} , was red shifted 17 nm upon protein addition, whereas the band broadened at the expense of the maximum intensity. We noted also that the bathochromic shift is larger as compared with the

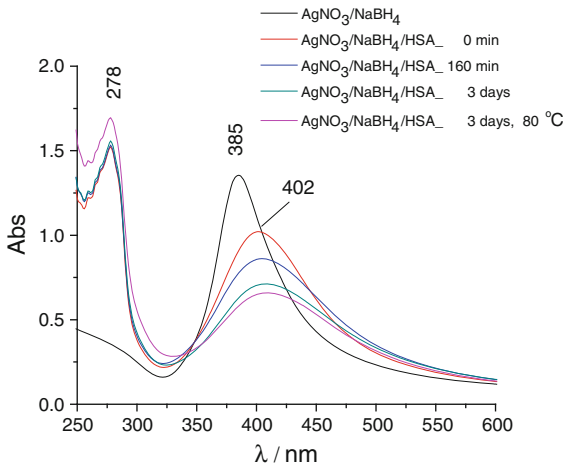


Fig. 3 UV-Vis absorption spectra of the HSA-Ag(0) nanoparticle complex as a function of reaction time and temperature. The concentration of HSA is 3.30×10^{-5} M

BSA-binding case. This feature may be attributed to different conformations and adsorbed amounts of the two proteins at the Ag(0) nanoparticle surface.

Meanwhile, the absorption spectra show that after 3 days and short-time thermal treatment at 80 °C, the absorption band at 278 nm increases with slightly blue-shift. The temperature effect could be considered responsible for this behavior.

Steady-state fluorescence analysis

The intrinsic fluorescence spectra of the BSA-Ag(0) nanoparticle complex were analyzed to evaluate the conformational changes around Trp residues. It is about of entire intrinsic fluorescence, of both Trp212 (deeply buried in the hydrophobic loop) and Trp134 (more exposed to hydrophilic environment) in BSA. According to the literature, the fluorescence emission of the native BSA, at an excitation wavelength of 279 nm, is 340 nm (Jung Se et al. 2006). Figure 4a shows the fluorescence emission spectra of the BSA-Ag(0) nanoparticle complex as a function of time. For an excitation wavelength of 280 nm, the fluorescence emission appears at 331 nm. At different reaction times, from 0 to 150 min, a quenching in the fluorescence of BSA was found. Even though no significant shifts in the maximum fluorescence emission were noted, a slight blue-shift was observed. This behavior means that the conformation around the Trp

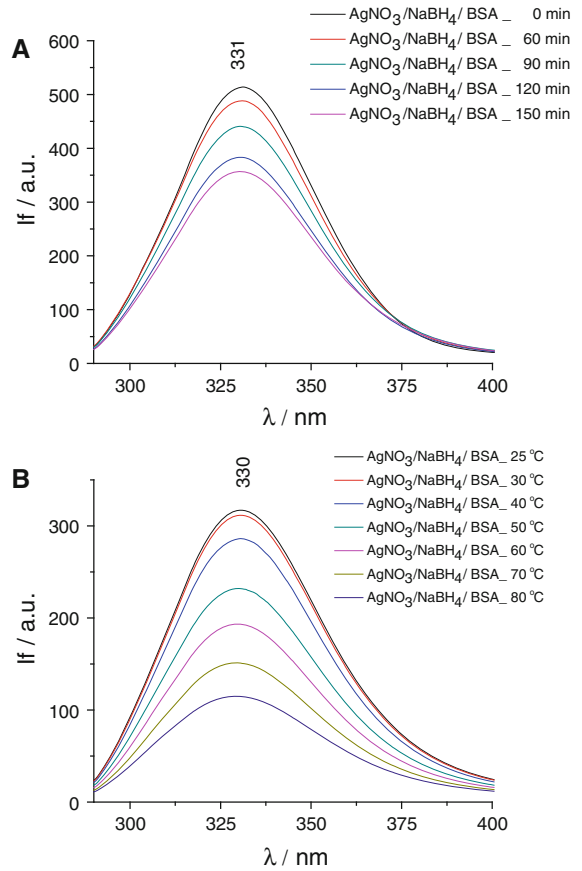


Fig. 4 Fluorescence emission spectra of the BSA-Ag(0) nanoparticle complex, at different reaction time (a) and different temperatures (b); BSA = 1.65×10^{-5} M, λ_{ex} = 280 nm

residues of the BSA-Ag(0) nanoparticle complex changes as compared to that of the native BSA.

It is known that the secondary structure of the BSA changed under thermal denaturation, the helicity of the protein (66 %) decreased with rise of temperature. Half of the original helicity is lost at 80 °C, while the helicity of 16 % is still maintained even at 130 °C (Moriyama et al. 2008). In these line, Fig. 4b, shows that the fluorescence intensity of BSA-Ag(0) nanoparticles complex, decreased gradually as the temperature increased from 25 to 80 °C. The fluorescence emission remained centered around 330 nm, exhibited a broad fluorescence band which was slightly blue-shifted.

Directly comparing with the free BSA, Fig. 5 presents the fluorescence emission spectra of the BSA-Ag(0) nanoparticle complex as a function of reaction time and temperature. As it can be seen, after

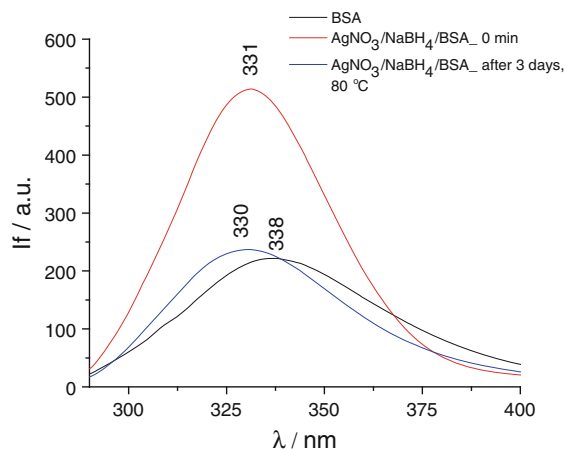


Fig. 5 Fluorescence emission spectra of the BSA–Ag(0) nanoparticle complex as a function of reaction time and temperature; $\lambda_{\text{ex}} = 280$ nm. The concentration of the free BSA is $1.8 \mu\text{M}$ and the concentration of BSA in the BSA–Ag(0) nanoparticles complex is 1.65×10^{-5} M

3 days and a short-time thermal treatment at 80°C , the fluorescence intensity is quenched and 8 nm red-shifted. For the control, the fluorescence emission of the BSA in the presence of the reducing agent (NaBH_4), was found at 335 nm. This means that BSA underwent conformational changes, causing less hydrophobic interaction with Ag(0) nanoparticles. Subsequently, the environment of the Trp residues changed due to the BSA–Ag(0) nanoparticle complex formation and(or) the temperature effect.

Figure 6 shows the fluorescence emission spectra of the HSA–Ag(0) nanoparticle complex at different temperatures. As can be observed, the fluorescence intensity gradually decreases as the temperature increases. Related to free HSA, of which the fluorescence emission appears at 333 nm, the maximum fluorescence emission wavelength is 8 nm blue-shifted, for the HSA–Ag(0) nanoparticle complex. The thermal denaturation of the HSA secondary structure is considered. Accordingly to Rezaei-Tavirani et al. 2006, the temperature increment from 25 to 55°C induces reversible conformational changes in the structure of HSA. As seen in the Fig. 6, the extent of the blue-shift is larger than in the case of the BSA–Ag(0) nanoparticle complex.

The fluorescence emission of the HSA in the presence of the reducing agent (NaBH_4) remains unchanged ($\lambda_{\text{em}} = 333$ nm), while the fluorescence emission of the HSA–Ag(0) nanoparticle complex, without thermal treatment, is 3 nm blue-shifted.

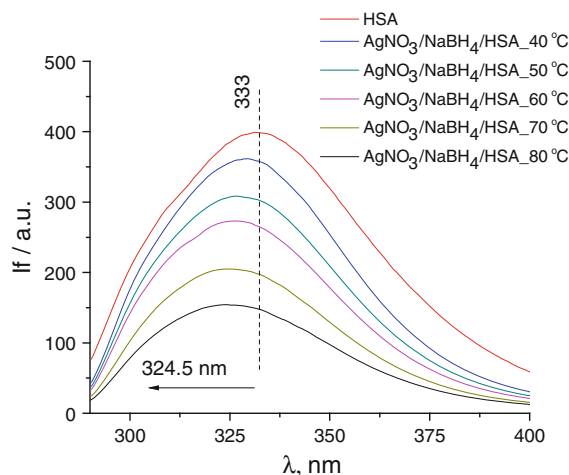


Fig. 6 Fluorescence emission spectra of the HSA–Ag(0) nanoparticles complex, at different temperatures; $\lambda_{\text{ex}} = 280$ nm. The concentration of the free HSA is $7 \mu\text{M}$ and the concentration of HSA in the HSA–Ag(0) nanoparticles complex is 3.30×10^{-5} M

Overall, the fluorescence quenching mechanism is supposed to be a dynamic one, which depends on the Trp residue location toward Ag(0) nanoparticle surface. This feature could be also corroborated with the nature of the interactions and hydrogen bondings and subsequently, an efficient quenching of the Trp takes place when HSA is adsorbed onto Ag(0) nanoparticles. According to the literature, the distance between Ag^+ and Trp is of 10 nm (Zhao et al. 2011). In line with this observation, the fluorescence quenching could be attributed to a micro-environmental hydrophilic effect of Trp residues of both BSA and HSA proteins on Ag(0) nanoparticles complex. Hence, an interaction between Ag and Trp is not taken into consideration.

Time-resolved fluorescence analysis

To corroborate the experimental results obtained by steady-state fluorescence analysis, time resolved fluorescence analysis was performed. It is known that by comparison with the static quenching process, only the dynamic quenching process reduces the fluorescence lifetimes. Fluorescence lifetime is an effective parameter to assess the quenching mechanism (Lakowicz 1999).

Fluorescence lifetimes of the HSA and BSA–Ag(0) nanoparticle complexes in direct comparison with free corresponding protein, are presented in Table 2. The fits were made with three and two components for HSA and BSA, respectively, considering the three

Table 2 Fluorescence lifetimes and pre-exponential factors of HSA and BSA proteins at their interaction with Ag (0) nanoparticles

Sample	α_1	τ_1 (ns)	α_2	τ_2 (ns)	α_3	τ_3 (ns)	$\langle\tau\rangle$ (ns)	χ^2
HSA/H ₂ O	0.088	0.369	0.009	2.726	0.010	6.559	4.15	1.272
HSA/NaBH ₄ /H ₂ O	0.113	0.335	0.008	2.239	0.008	6.207	3.424	1.145
HSA/NaBH ₄ /AgNO ₃	0.129	0.310	0.007	1.759	0.006	5.803	2.710	1.234
BSA/H ₂ O	0.074	0.520	0.013	5.124	–	–	3.438	1.360
BSA/NaBH ₄ /H ₂ O	0.079	0.566	0.011	3.919	–	–	2.211	1.389
BSA/NaBH ₄ /AgNO ₃	0.100	0.494	0.007	4.043	–	–	1.787	1.469

The compound concentration is 3.29×10^{-5} M; $\lambda_{ex} = 295$ nm; χ^2_R presents the quality of the fit; the residuals goodness of the fit values were determined for 2 and 3 component fits

rotamers of Trp214 in HSA (Rolinski et al. 2008; Amiri et al. 2010) and the two Trp residues in BSA (Johansson 1997; De-Llanos et al. 2011). As it can be seen, the average fluorescence lifetimes of both HSA/BSA–Ag(0) nanoparticles complexes decreases dramatically: from 4.15 ns for free HSA to 2.71 ns when the complex is formed and from 3.43 ns for free BSA to 1.78 ns in the complex. For comparison, the fluorescence lifetime value for BSA–Ag(0) nanoparticles complex (1.78 ns) is lower than the fluorescence lifetime value of HSA–Ag(0) nanoparticles complex (2.71 ns). This can be explained as follows. As, unlike HSA, BSA has two Trp residues, one buried in the protein, Trp212, and the other on its surface, Trp134, the presence of the nanoparticles influences to a larger extent the emission properties of Trp134, both the intensity and the lifetime (Liu et al. 2009).

Circular dichroism analysis

To further investigate the conformational changes of the BSA and HSA proteins adsorbed onto Ag(0) nanoparticles, circular dichroism studies were carried out. It was reported that the Ag nanoparticles obtained by the citrate method and with average dimensions of

Table 3 Percentage of the secondary structure elements of the HSA and BSA proteins at their interaction with Ag (0) nanoparticles

Sample	α -Helix (%)	β -Sheet (%)	Random coil (%)
HSA/H ₂ O	68.25	11.26	20.49
HSA/NaBH ₄ /AgNO ₃	65.46	12.10	22.43
BSA/H ₂ O	59.87	16.90	23.23
BSA/NaBH ₄ /AgNO ₃	50.30	23.44	26.25

The proteins concentration is 0.044 mg/mL

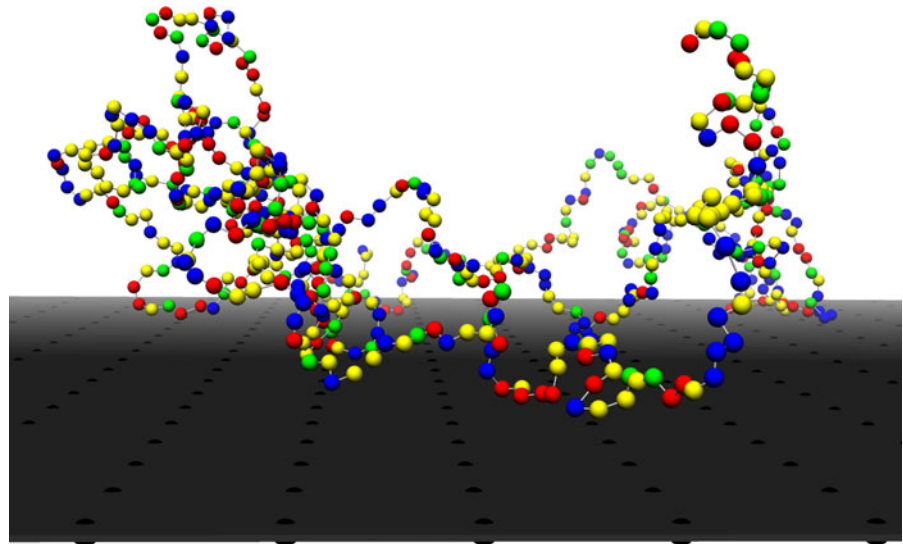
40–50 nm could increase the amount of helix and decrease the beta sheet structure leading to a loosening of the native protein structure. In the loose structure, internal hydrophobic amino acids are exposed and the characteristic fluorescence of BSA is obviously quenched. BSA distorted the double-layer structure of nanoAg and covered its surface, generating a BSA–nanoAg complex held together by van der Waals and electrostatic forces (Shaikh et al. 2007). Also, Ag⁺ sites bound to the aminoacid residues of the backbone chain of BSA, destroyed the hydrogen bonding networks and further caused partial unfolding of protein (Zhao et al. 2011; Shaikh et al. 2007).

Table 3 presents the percentage of the secondary structure elements of the BSA and HSA into Ag(0) nanoparticle complexes. It can be observed that the change of the secondary structure is slightly different for both BSA and HSA proteins at their interaction with Ag(0) nanoparticles. In direct comparison with the native BSA (59.87 % α -helix) in the BSA–Ag(0) nanoparticles complex, the secondary structure of BSA underwent a decrease in α -helix (50.3 %), while the β -sheet and random-coil structures increased. On the contrary, for HSA–Ag(0) nanoparticles complex, the secondary structure elements, the α -helix, β -sheet as well as random-coil structures, underwent slight changes. Hence, the backbone of the BSA and HSA proteins in protein–Ag(0) nanoparticle complex depends on a different protein denaturation. Comparing our results with those of (Liu et al. 2009), it also seems that the nature of the nanoparticles influences the denaturation process.

Model system and Monte Carlo simulations details

A simulation snapshot exhibiting the equilibrium configuration of the HSA protein chain at the Ag

Fig. 7 Snapshot illustrating the conformation adopted by the HSA chain at the positively charged, flat surface. Color code: negatively charged (*red*), positively charged (*green*), neutral (*blue*), and hydrophobic amino acids (*yellow*); the *black dots* onto the flat surface stand for the location of its positive charges. The small ions were omitted for the sake of clearer view of the amino acid positions. (Color figure online)



positively charged surface is displayed in Fig. 7. The protein chain appears to be relatively in-plane extended with no section stretching away from the surface. Moreover, all four types of the amino acid were found next to the surface. The conformational analysis revealed that protein chain underwent a stretching when being adsorbed. Thus, the root-mean-square (rms) radius of gyration, $\langle R_G^2 \rangle^{1/2}$ increased from 97 to 128 Å, and the ratio of the rms end-to-end distance and gyration radius, $r = \langle R_{ce}^2 \rangle / \langle R_G^2 \rangle$, increased from 4.8 to 6.3 upon chain adsorption. We mention that a more extended protein configuration leads to an enhancement of both quantities, yet they depend differently on the shape. The chain shape is particularly quantified by the latter parameter, which reaches the particular values $r \sim 6$ for a Gaussian chain and $r \sim 12$ in the rodlike limit.

The distribution of the different types of amino acids, N_{aa} , perpendicular to the surface (z direction) is shown in Fig. 8. In line with the snapshot displayed in Fig. 7, the amino acid numbers near the surface were different from zero. Notably, the functional forms of amino acid numbers were similar, denoting that the electrostatic interactions between the protein chain and the oppositely charged surface did not result in a separation between the negatively charged and the positively charged amino acid. Nevertheless, the maximum in the bead number profile took place at slightly different distances away from the surface. Thus, the maximum amino acid number was reached at $z = 15$ Å and $z = 28$ Å for negatively and

positively charged beads, respectively. It is also noted that both neutral and hydrophobic beads accumulated at $z \sim 23$ Å.

When the distribution of a single bead, in particular the fluorescent neutral Trp amino acid, $N_{Trp}(z)$, was compared with the averaged distribution of the different types of amino acids, a prominent change was noticed (Fig. 8). We noticed that Trp bead is depleted from the surface as $N_{Trp} \sim 0$ at $z < 15$ Å and shifted away from the surface as a broad

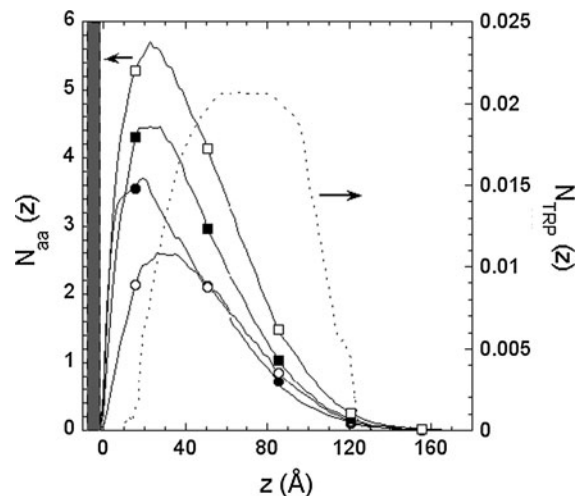


Fig. 8 Number distribution in the z direction, $N_{aa}(z)$, for the negatively charged (*filled circle*), positively charged (*open circle*), neutral (*filled square*), and hydrophobic (*open square*) amino acids. Trp-residue distribution, $N_{Trp}(z)$, is also shown (*dotted curve*). The *gray box* represents the surface location

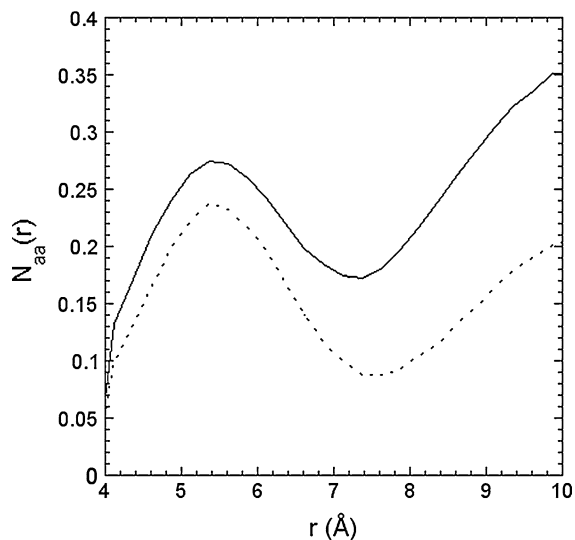


Fig. 9 Radial number of amino acids of the free (*continuous curve*) and adsorbed (*dashed curve*) HSA chain; $r = 0$ Å is the centre of Trp bead

maximum at $55 \text{ \AA} < z < 87 \text{ \AA}$. The former feature suggests that the surface charges could not interfere in the collisional quenching of the Trp fluorescence, whereas the latter one hints at a water exposure of the Trp bead upon adsorption. This assumption is supported by the fact that the amino acids number around the Trp bead decreased as a result of complexation, as shown in Fig. 9. We then infer that the HSA chain section surrounding the Trp bead adopted a more opened structure upon adsorption, which in turn would result in the quenched Trp fluorescence experimentally found.

Conclusion

At the interaction with Ag(0) nanoparticles, both BSA and HSA fluorescence was quenched by a dynamic quenching process, and the fluorescence emission spectrum indicated conformational changes of the protein sections containing Trp residues. In addition, upon adsorption, the location of the Trp residues with respect to the nanoparticle surface is different in BSA/HSA–Ag(0) nanoparticles complex and hence, changes into the functional properties of the serum albumins appear.

The fluorescence quenching of the Trp residues was found to be temperature dependent: more efficiently in the case of the BSA–Ag(0) nanoparticles complex

than that in the case of HSA–Ag(0) nanoparticles complex. A strong blue-shift fluorescence emission (8 nm) for the HSA–Ag(0) nanoparticles complex was evidenced.

The secondary structure for both BSA and HSA proteins slightly changed at the interaction with Ag(0) nanoparticles. The protein backbone depends on micro-environmental denaturation.

The overall protein conformation upon adsorption on nanoparticle's surface is an opened one which in turn results in the quenched Trp fluorescence.

The assumption of a more hydrophilic microenvironment of the Trp residue upon HSA adsorption is supported by the simulations data which also revealed that the surface charges did not interfere with the collisional quenching of the Trp fluorescence.

Acknowledgments This study has been performed in the frame of the Romanian Academy programme and II. 8 theme of the INFRANANOCHEM Project. DA acknowledges the use of the HPC infrastructure developed under NASR Grant, Capacities Project CpI 84/2007. The authors are indebted to Dr. Valentin S. Teodorescu for Transmission Electron Microscopy.

References

- Abdullin TI, Bondar OV, Shtyrlin YG et al (2010) Pluronic block copolymer-mediated interactions of organic compounds with noble metal nanoparticles for SERS analysis. *Langmuir* 26:5153–5159
- Akinchina A, Linse P (2002) Monte Carlo simulations of polyion–macroion complexes. 1. Equal absolute polyion and macroion charges. *Macromolecules* 35:5183–5193
- Alivisatos AP (2004) The use of nanocrystals in biological detection. *Nat Biotechnol* 22:47–52
- Allara D (1995) In: Ulman A (ed) *Characterization of organic thin films*. Butterworth-Heinemann, Boston
- Amendola V, Bakr OM, Stellacci F (2010) A study of the surface plasmon resonance of silver nanoparticles by the discrete dipole approximation method: effect of shape, size, structure, and assembly. *Plasmonics* 5:85–97
- Amiri M, Jankeje K, Albani JR (2010) Origin of fluorescence lifetimes in human serum albumin. studies on native and denatured protein. *J Fluoresc* 20:651–656
- Angelescu DG, Stenhammar J, Linse P (2007) Packaging of a flexible polyelectrolyte inside a viral capsid: effect of salt concentration and salt valence. *J Phys Chem B* 111: 8477–8485
- Angelescu DG, Vasilescu M, Somoghi R et al (2010) Kinetics and optical properties of the silver nanoparticles in aqueous L64 block copolymer solutions. *Colloid Surf A* 366:155–162
- De-Llanos R, Sánchez-Cortes S, Domingo C et al (2011) Surface plasmon effects on the binding of antitumoral drug emodin to bovine serum albumin. *J Phys Chem C* 115: 12419–12429

- Elghanian R, Storhoff JJ, Mucic RC et al (1997) Selective colorimetric detection of polynucleotides based on the distance-dependent optical properties of gold nanoparticles. *Science* 277:1078–1080
- El-Sayed IH, Huang X, El-Sayed MA (2005) Surface plasmon resonance scattering and absorption of anti-egfr antibody conjugated gold nanoparticles in cancer diagnostics: applications in oral cancer. *Nano Lett* 5:829–834
- El-Sayed IH, Huang X, El-Sayed MA (2006) Selective laser photo-thermal therapy of epithelial carcinoma using anti-EGFR antibody conjugated gold nanoparticles. *Cancer Lett* 239:129–135
- Esumi K, Matsushima Y, Torigoe K (1995) Preparation of rod-like gold particles by UV irradiation using cationic micelles as a template. *Langmuir* 11:3285–3287
- Evans TW (2002) Review article: albumin as a drug-biological effects of albumin unrelated to oncotic pressure. *Aliment Pharmacol Ther* 16:6–11
- Furno F, Morley KS, Wong B et al (2004) Silver nanoparticles and polymeric medical devices; a new approach to prevention of infection? *J Antimicrob Chemother* 54:1019–1024
- Gu H, Xu K, Xu C, Xu B (2006) Biofunctional magnetic nanoparticles for protein separation and pathogen detection. *Chem Commun* 7(9):941–946
- Haes AJ, Van Duyne RP (2002) A nanoscale optical biosensor: sensitivity and selectivity of an approach based on the localized surface plasmon resonance spectroscopy of triangular silver nanoparticles. *J Am Chem Soc* 124:10596–10604
- Hansen UK (1981) Molecular aspects of ligand binding to serum albumin. *Pharmacol Rev* 33:17–53
- Hayat MA (1991) Colloidal gold: principles, methods, and applications. Academic Press, San Diego
- Hostetler MJ, Templeton AC, Murray RW (1999) Dynamic of place-exchanged reactions on monolayer-protected gold cluster molecules. *Langmuir* 15:3782–3789
- Huang X, El-Sayed IH, Qian W et al (2006) Cancer cell imaging and photothermal therapy in the near-infrared region by using gold nanorods. *J Am Chem Soc* 128:2115–2120
- Huang X, Jain PK, El-Sayed IH et al (2007) Gold nanoparticles: interesting optical properties and recent applications in cancer diagnostics and therapy. *Nanomedicine* 2:681–693
- Huo Q (2007) A perspective on bioconjugated nanoparticles and quantum dots. *Colloid Surf B Biointerf* 59:1–10
- Ingram RS, Hostetler MJ, Murray RW (1997) Poly-hetero- ω -functionalized alkanethiolate-stabilized gold cluster compound. *J Am Chem Soc* 119:9175–9178
- Jain PK, Lee KS, El-Sayed IH et al (2006) Calculated absorption and scattering properties of gold nanoparticles of different size, shape, and composition: applications in biological imaging and biomedicine. *J Phys Chem B* 110:7238–7248
- Jain PK, Huang W, El-Sayed MA (2007a) On the universal scaling behavior of the distance decay of plasmon coupling in metal nanoparticles pairs: a plasmon rule equation. *Nano Lett* 7(7):2080–2088
- Jain PK, El-Sayed IH, El-Sayed MA (2007b) Au nanoparticles target cancer. *Nano Today* 2:18–29
- Jain PK, Huanh X, El-Sayed IH et al (2008) Noble metals on the nanoscale: optical and photothermal properties and some applications in imaging, sensing, biology, and medicine. *Acc Chem Res* 41(12):1578–1586
- Jensen PS, Chi Q, Grumens FB et al (2005) Gold nanoparticles assisted assembly of a heme protein for enhancement of long-range interfacial electron transfer. *J Phys Chem C* 111:6124–6132
- Johansson JS (1997) Binding of the volatile anesthetic chloroform to albumin demonstrated using tryptophan fluorescence quenching. *J Biol Chem* 272:17961–17965
- Jonsson M, Skepo M, Tjerneld F et al (2003) Effect of spatially distributed hydrophobic surface residues on protein-polymer association. *J Phys Chem B* 107:5511–5518
- Jung Se H, Choi SJ, Kim HJ et al (2006) Molecular characteristics of bovine serum albumin-dextran conjugates. *Biosci Biotechnol Biochem* 70:2064–2070
- Lakowicz JR (1999) Principles of fluorescence spectroscopy, 2nd edn. Kluwer Academic Publishers, Dordrecht
- Lakowicz JR, Kusba J, Shen Y et al (2003) Effect on metallic silver particles on resonance energy transfer between fluorophores bound to DNA. *J Fluoresc* 13:69–77
- Li Y, Leung P, Yao L et al (2006) Antimicrobial effect of surgical masks coated with nanoparticles. *J Hosp Infect* 62:58–63
- Link S, El-Sayed MA (2000) Shape and size dependence of radiative, non-radiative and photothermal properties of gold nanocrystals. *Internat Rev Phys Chem* 19:409–453
- Link S, Mohamed MB, El-Sayed MA (1999) Simulation of the optical absorption spectra of gold nanorods as a function of their aspect ratio and the effect of the medium dielectric constant. *J Phys Chem B* 103:3073–3077
- Linse P (2009) MOLSIM ver. 4.13, Lund University, Sweden
- Liu R, Sun F, Zang L et al (2009) Evaluation on the toxicity of nanoAg to bovine serum albumin. *Sci Total Environ* 407:4184–4188
- Lund M, Jönsson B (2003) A mesoscopic model for protein-protein interactions in solution. *Biophys J* 85:2940–2947
- Mariam J, Dongre PM, Kothari DC (2011) Study of interaction of silver nanoparticles with bovine serum albumin using fluorescence spectroscopy. *J Fluoresc* 21:2193–2199
- Moreno F, Cortijo M, Jimenez JG (1999) Interaction of acrylodan with human serum albumin. A fluorescence spectroscopic study. *Photochem Photobiol* 70:695–700
- Moriyama Y, Watanabe E, Kobayashi K et al (2008) Secondary Structural Change Of Bovine Serum Albumin In Thermal Denaturation up to 130 °C and protective effect of sodium dodecyl sulfate on the change. *J Phys Chem B* 112:16585–16589
- Naja G, Bouvrette P, Champagne J et al (2010) Activation of nanoparticles by biosorption for *E. coli* detection in milk and apple juice. *Appl Biochem Biotechnol* 162:460–475
- Niemeyer CM (2001) Nanoparticles, proteins and nucleic acids: biotechnology meets materials science. *Angew Chem Int Ed* 40:4128–4158
- O'Neal DP, Hirsch LR, Halas NJ et al (2004) Photo-thermal tumor ablation in mice using near infrared-absorbing nanoparticles. *Cancer Lett* 209:171–176
- Olson RE, Christ DD (1996) Plasma protein binding of drugs. *Ann Rep Med Chem* 31:327–336
- Ravindran A, Singh A, Raichur AM et al (2010) Studies on interaction of colloidal Ag nanoparticles with bovine serum albumin (BSA). *Colloids Surf B* 76:32–37

- Reinhard B, Sheikholeslami S, Mastroianni A et al (2007) Use of plasmon coupling to reveal the dynamics of DNA bending and cleavage by single ecorv restriction enzymes. *Proc Natl Acad Sci USA* 104:2667–2672
- Rezaei-Tavirani M, Moghaddamnia SH, Ranjbar B et al (2006) Conformational study of human serum albumin in pre-denaturation temperatures by differential scanning calorimetry, circular dichroism and UV spectroscopy. *J Biochem Mol Biol* 39:530–536
- Roach P, Farrar D, Perry C (2006) Surface tailoring for controlled protein adsorption: effect of topography at the nanometer scale and chemistry. *J Am Chem Soc* 128:3939–3945
- Rolinski OJ, Martin A, Birch DJS (2008) Human serum albumin-flavonoid interactions monitored by means of tryptophan kinetics. *Ann NY Acad Sci* 1130:314–319
- Rosi NL, Mirkin CA (2005) Nanostructures in biodiagnostics. *Chem Rev* 105:1547–1562
- Rupp B, CDfit. <http://www.ruppweb.org/Xray/comp/cdfit.htm>
- Samoshima Y, Nylander T, Shubin V et al (2005) Equilibrium aspects of polycation adsorption on silica surface: how the adsorbed layer responds to changes in bulk solution. *Langmuir* 21:5872–5881
- Shaikh SMT, Seetharamappa J, Kandagal PB et al (2007) Spectroscopic investigations on the mechanism of interaction of bioactive dye with bovine serum albumin. *Dye Pigment* 74:665–671
- Shrivastava S, Bera T, Singh SK et al (2009) Characterization of antiplatelet properties of silver nanoparticles. *ACS Nano* 3(6):1357–1364
- Skepo M, Linse P, Arnebrant T (2006) Coarse-grained modeling of proline rich protein 1 (PRP-1) in bulk solution and adsorbed to a negatively charged surface. *J Phys Chem B* 110:12141–12148
- Sokolov K, Follen M, Aaron J et al (2003) Real-time vital optical imaging of precancer using anti-epidermal growth factor receptor antibodies conjugated to gold nanoparticles. *Cancer Res* 63:1999–2004
- Sönnichsen C, Reinhard BM, Liphardt J et al (2005) Molecular ruler based on plasmon coupling of single gold and silver nanoparticles. *Nat Biotechnol* 23:741–745
- Sudlow G, Birkett DJ, Wade DN (1976) Further characterization of specific drug binding sites on human serum albumin. *Mol Pharmacol* 12(6):1052–1061
- Templeton AC, Hostetler MJ, Kraft CT et al (1998) Reactivity of monolayer-protected gold cluster molecules: steric effects. *J Am Chem Soc* 120:1906–1911
- Templeton AC, Wuelfing WP, Murray RW (2000) Monolayer-protected cluster molecules. *Acc Chem Res* 33:27–36
- Tian J, Wong K, Ho C et al (2007) Topical delivery of silver nanoparticles promotes wound healing. *Chem Med Chem* 2:129–136
- Tozzini V (2005) Coarse-grained models for proteins. *Curr Opin Struct Biol* 15:144–150
- Ulman A (1991) *Ultrathin organic films*, 1st edn. Academic Press, San Diego
- Ulman A (1996) Formation and structure of self-assembled monolayers. *Chem Rev* 96:1533–1554
- Valanciunaite J, Bagdonas S, Streckyte G et al (2006) Spectroscopic study of TPPS₄ nanostructures in the presence of bovine serum albumin. *Photochem Photobiol Sci* 5:381–388
- Voicescu M, Heinrich M, Hellwig P (2009a) Steady-state and time resolved fluorescence analysis of tyrosine–histidine model compounds. *J Fluoresc* 19:257–266
- Voicescu M, El Khoury Y, Martel D et al (2009b) Spectroscopic analysis of tyrosine derivatives: on the role of the tyrosine–histidine covalent linkage in cytochrome c oxidase. *J Phys Chem B* 113:13429–13436
- Wang H, Xu K, Liu L et al (2010) The efficacy of self-assembled cationic antimicrobial peptide nanoparticles against *Cryptococcus neoformans* for the treatment of meningitis. *Biomaterials* 31:2874–2881
- Willner L, Baron R, Willner B (2007) Integrated nanoparticles-biomolecule systems for biosensing and bioelectronics. *Biosens Bioelectron* 22:1841–1852
- Zhao X, Liu R, Teng Y et al (2011) The interaction between Ag⁺ and bovine serum albumin: a spectroscopic investigation. *Sci Total Environ* 409:892–897